Science Advances | AAAS
SIGNIFICANT RESEARCH, GLOBAL IMPACT

Sci Adv. 2022 Mar 18;8(11):eabn0485. doi: 10.1126/sciadv.abn0485

Piezo1 regulates the regenerative capacity of skeletal muscles via orchestration of stem cell morphological states

Nuoying Ma [1,2], Delia Chen [1], Ji-Hyung Lee [1], Paola Kuri [3], Edward Blake Hernandez [1], Jacob Kocan [1], Hamd Mahmood [1], Elisia D Tichy [1], Panteleimon Rompolas [3,4], Foteini Mourkioti [1,4,5,*]

Author information Article notes Copyright and License information

PMCID: PMC8932657 PMID: 35302846

Abstract

Muscle stem cells (MuSCs) are essential for tissue homeostasis and regeneration, but the potential contribution of MuSC morphology to in vivo function remains unknown. Here, we demonstrate that quiescent MuSCs are morphologically heterogeneous and exhibit different patterns of cellular protrusions. We classified quiescent MuSCs into three functionally distinct stem cell states: responsive, intermediate, and sensory. We demonstrate that the shift between different stem cell states promotes regeneration and is regulated by the sensing protein Piezo1. Pharmacological activation of Piezo1 is sufficient to prime MuSCs toward more responsive cells. Piezo1 deletion in MuSCs shifts the distribution toward less responsive cells, mimicking the disease phenotype we find in dystrophic muscles. We further demonstrate that Piezo1 reactivation ameliorates the MuSC morphological and regenerative defects of dystrophic muscles. These findings advance our fundamental understanding of how stem cells respond to injury and identify Piezo1 as a key regulator for adjusting stem cell states essential for regeneration.

Piezo1 regulates functional mechanoproperties of muscle stem cells during regeneration.

INTRODUCTION

The ability of cells to communicate with their microenvironment and coordinate their activity is fundamentally important in multicellular organisms both during tissue development and homeostasis. In addition, while we know more about interactions between ligands and receptors in a cell (*1*), we know less about how the right type of cells respond to the right type of signals in a more complex environment [discussed in (*2*)]. In recent years, mechanical stimuli, stiffness, and filopodia have emerged as a mean of influencing cell behavior either in vitro or among various organisms in vivo (*2*–*6*). Yet, we have a limited mechanistic understanding of how stem cells sense their local microenvironment to control maintenance, shape biological processes, and repair tissues.

Skeletal muscles have a remarkable capacity to regenerate, due to the presence of adult progenitor cells, called muscle stem cells (MuSCs; also known as satellite cells), which have the ability to self-renew, restore, and repair damaged myofibers (*7*). Therefore, studying MuSCs has been an informative stem cell mammalian model system over the years to understand how stem cell behavior and plasticity can be altered in response to injury and other tissue signals (*8*). MuSCs lie in a quiescent state on the surface of the muscle fiber between the basal lamina and the sarcolemma (*9*). Pax7 is the most used marker of adult MuSCs (*8*), and $Pax7^{+}$ cells are both necessary and sufficient for adult muscle repair (*10*). MuSC function is severely affected in chronic muscle diseases, such as in Duchenne muscular dystrophy (DMD) (*11*–*14*). Since their discovery 60 years ago (*9*), much has been learned regarding the role of MuSCs in homeostasis, regeneration, and disease. The potential function of MuSCs during development, and their proximity to capillaries in adult muscles (*15*), and the need for ghost fibers to promote differentiation of myogenic progenitors in mice (*16*) have provided further insights. However, with a few recent exceptions (*15*–*17*), the majority of MuSC studies use either histological analysis of skeletal muscle sections (*3*, *12*, *17*–*20*) or single-fiber isolation procedures ex vivo (*21*–*23*), both of which disrupt muscle integrity. As a result, the potential functional contribution of MuSC morphology to muscle homoeostasis and its regulation during regeneration and disease in intact adult muscles remain unknown.

To assess MuSC structural complexity and performance within their natural environment, we generated a mouse model that permits their visualization in unperturbed mouse muscles at the single-cell level (*17*). We found that adult MuSCs in their endogenous position are a morphologically heterogeneous population and exhibit sophisticated, cellular axon-like protrusions that extend across and along the muscle fiber and differ in number and length, even under quiescence. We found that dynamic regulation of these protrusions coincides with a transition between the different functional phases of muscle regeneration, with cells with less protrusions being more adaptive and the first to respond to injury, while cells with more protrusions are more dormant and reduce their protrusion length at a later phase of regeneration. Our data reveal that differential protrusion number, length, and complexity are associated with distinct MuSC functional subtypes and that these protrusions are used to decipher the microenvironment and coordinate the function of MuSCs during muscle regeneration.

The impact of microenvironmental stiffness on MuSC activation (*5*) as well as the importance of mechanoregulation of

stem cells across different contexts from development to differentiation are becoming increasingly appreciated (*3*, *4*, *24*). Emerging evidence in other fields implicates an interplay between the mechanosensing pathway Piezo1 and the cytoskeleton to modulate physiological processes (*25*). Piezo1 is an important mediator of various aspects of mechanotransduction and mediates cell fate determination in mesenchymal stem cells (*26*) and osteoblasts (*27*). However, it is currently unknown whether Piezo1 can regulate MuSC morphology, remodeling, and function. Here, we explored these principles with regard to MuSCs, investigated the effects of pharmacological activation of Piezo1 on MuSC heterogeneity, and generated Piezo1 conditional MuSC knockout mice. We found that Piezo1 defines MuSC subtypes and coordinates the MuSC transition toward cells with less protrusions in homeostasis and regeneration. The physiological importance of our findings was further highlighted by our demonstration that, in muscular dystrophy, protrusion length is aberrantly regulated, Piezo1 levels are low, and the number of cells with few protrusions is reduced. Pharmacological reactivation of Piezo1 ameliorates the aberrant morphology of diseased MuSCs and boosts muscle regeneration in dystrophic mice. Therefore, MuSCs have protrusions that establish their stem cell state and Piezo1 is necessary for their transition toward more activated stem cell forms, such as the ones that are impaired in diseased conditions.

RESULTS

Quiescent MuSCs exhibit variability in protrusions within their natural environment

While previous histological and single-fiber isolation data have been extensively used to study MuSCs, the full range of morphological properties of stem cell populations has not been directly characterized in vivo. We recently generated a Pax7EGFP reporter mouse that uses the endogenous Pax7 promoter to drive expression of enhanced green fluorescent protein (EGFP) and demonstrated that Pax7-driven EGFP is a dynamic marker of MuSC stemness in vitro (*17*). To further characterize MuSCs in their endogenous location, the hindlimb tibialis anterior (TA) muscles were visualized by two-photon microscopy to identify $EGFP^+$ quiescent MuSCs, while muscle fibers were assessed by second-harmonic generation (SHG) imaging of sarcomeres (Fig. 1A). We found that quiescent MuSCs do not exist as round cells in vivo but instead exhibit elongated axon-like cytoplasmic extensions that we termed “protrusions,” which vary in number and length (Fig. 1B and movie S1). Most of the MuSCs have two protrusions (Fig. 1C); however, a significant number of cells have 0, 1, 3, 4, or ≥5 (Fig. 1, B and C). Notably, when MuSCs are isolated from the Pax7EGFP muscles, protrusions are no longer visible (fig. S1A), suggesting that these structures disassemble quickly in response to skeletal muscle disruption. Further characterization of EGFP-expressing Pax7 cells within skeletal muscles revealed that while 86% of these MuSCs have nonbranching protrusions, the remaining 14% have one, two, and sometimes three or more branches (Fig. 1, D and E). In addition, the total protrusion length is positively correlated with the increase in the number of protrusions per cell (Fig. 1F). Together, these data demonstrate that quiescent MuSCs are a morphologically heterogeneous population in vivo. To reveal the spatial placement of the “axon-like” MuSCs on muscle fibers, we quantified the orientation of cells and found that MuSCs with zero and one protrusions tend to align parallel across the muscle fiber. As the number of protrusions increases, cells change their orientation and tend to align more

perpendicularly to the myofiber (Fig. 1G). These data provide direct evidence that quiescent MuSCs do not uniformly align across the fiber in their endogenous environment, adding another layer of topological heterogeneity to adult MuSCs.

Fig. 1. Adult MuSCs are a morphologically heterogeneous population in vivo.

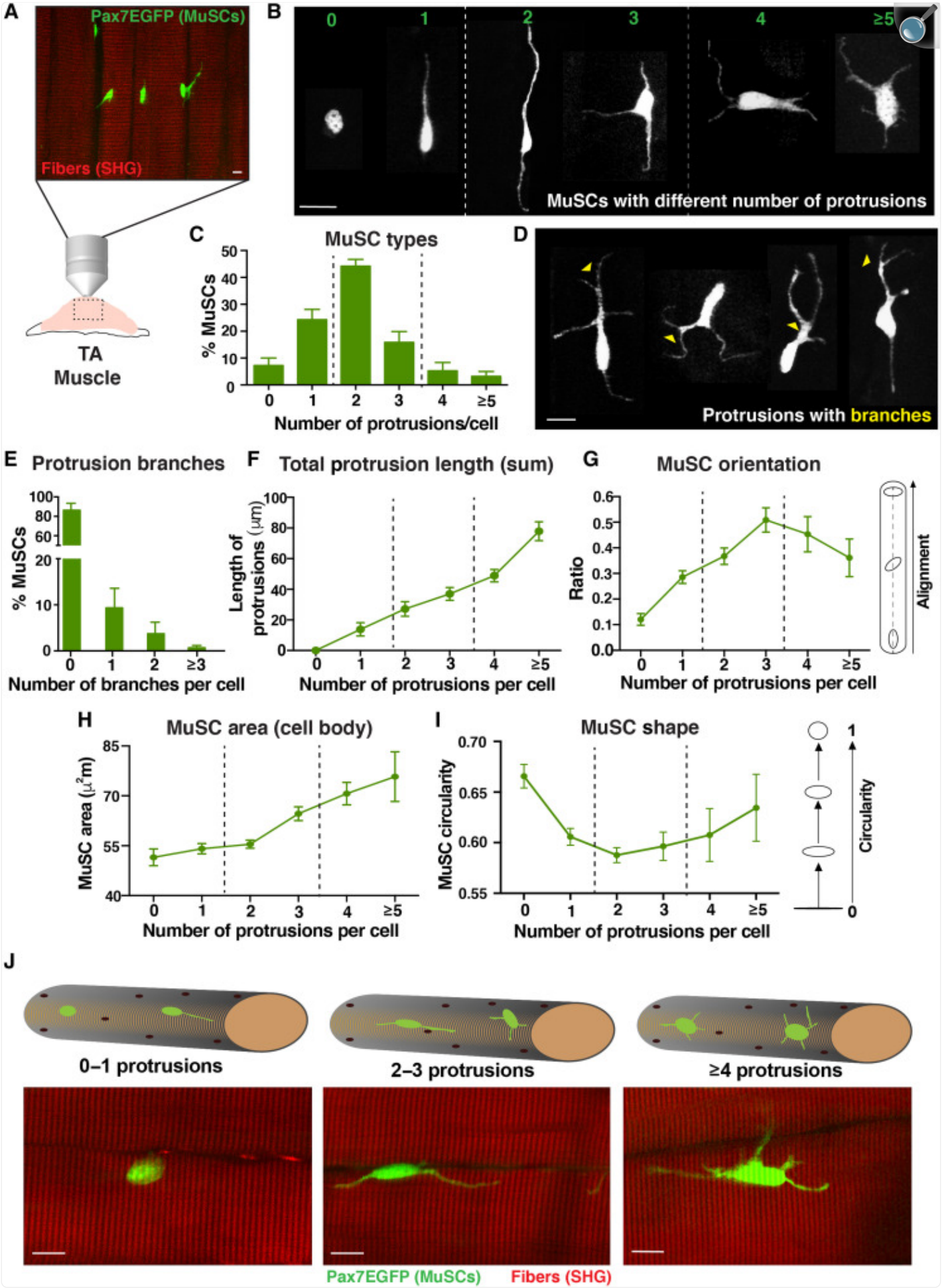
A
Pax7EGFP (MuSCs)
Fibers (SHG)
TA
Muscle
B
0
1
2
3
4
≥5
MuSCs with different number of protrusions
C
MuSC types
% MuSCs
Number of protrusions/cell
D
Protrusions with branches
E
Protrusion branches
% MuSCs
Number of branches per cell
F
Total protrusion length (sum)
Length of protrusions (μm)
Number of protrusions per cell
G
MuSC orientation
Ratio
Alignment
Number of protrusions per cell
H
MuSC area (cell body)
MuSC area (μ²m)
Number of protrusions per cell
I
MuSC shape
MuSC circularity
Circularity
Number of protrusions per cell
J
0–1 protrusions
2–3 protrusions
≥4 protrusions
Pax7EGFP (MuSCs)
Fibers (SHG)

Open in a new tab

(**A**) Schematic representation of TA muscle imaging using two-photon microscopy. MuSCs are green (EGFP), and sarcomeres are marked by SHG in red. Scale bar, 10 μm. (**B**) Representative images of quiescent MuSCs with zero, one, two, three, four, and five or more protrusions. Scale bar, 10 μm. (**C**) Quantification of MuSCs with different numbers of protrusions shows that the majority of cells have two protrusions, followed by cells with one and three; $n = 3$ mice (2 months old; both legs, a total of six TA adult muscles); $N > 600$ cells per muscle were analyzed. (**D**) Representative images of quiescent MuSCs with branched protrusions. Scale bar, 10 μm. (**E**) Analysis shows that the majority of MuSCs have protrusions with no branches (0) and only a small percentage of cells have branches. (**F**) Total sum protrusion length is correlated with the increased number of protrusions per cell. (**G**) Orientation analysis of MuSCs shows that not all cells are aligned the same. Schematic representation of the cell alignment is shown on the right. (**H**) MuSC area quantification shows that cells are larger as the number of protrusions increases. (**I**) Analysis of nuclear shape of quiescent MuSCs. Nuclear shape ranges from a line (0) up to a complete circle (1), as shown on the right of the graph. (**J**) Schematic representation (top) and representative images (bottom) of three examples of quiescent MuSC subtypes. Scale bars, 10 μm.

Protrusions from other cell types are thought to mediate local communication between adjacent cells through physical contact (*2*, *15*). To investigate whether MuSC protrusions extend to other nuclei on the fiber, we generated a mouse (Pax7EGFP; RosanTnG) in which muscles bear green MuSCs (EGFP) and red nuclei (tdTomato) (fig. S1B). Notably, we observed that the vast majority of cells with one and two protrusions are in close proximity to other nuclei on the fiber (fig. S1C). However, the cells with more than four protrusions rarely reside near nuclei, but instead, their protrusions extend across and along the sarcomeres of the muscle fiber. These data suggest that cells with fewer than three protrusions likely participate in cell-to-cell communication, while cells with four or more protrusions extend toward the muscle fiber, possibly "sensing" the muscle environment. We also found that MuSCs with an increased number of protrusions have a larger surface area (Fig. 1H), while MuSCs with zero protrusions are more circular (Fig. 1I). These data suggest that the increased number of protrusions is used by quiescent cells in uninjured conditions to probe the muscle environment. Similar MuSC distribution and protrusion metrics were observed whether we looked in the middle of TA (Fig. 1) or the muscle area close to the tendon (TA myotendinous area; fig. S2, A to F). Moreover, analysis of the Pax7EGFP soleus muscle showed similar MuSC and protrusion distribution (fig. S2, G to L), suggesting that these parameters do not vary considerably between fast-twitch and slow-twitch leg muscles under steady-state conditions. Overall, this comprehensive characterization of cells in quiescence (Fig. 1J) establishes an original framework to study the function of MuSCs in their native environment following injury of healthy muscles as well as in degenerating diseased muscles before and after therapeutic treatment.

Cellular protrusions in adult uninjured muscles are not used to mobilize MuSCs

Cellular protrusions in other cell types, including cancer cells undergoing metastasis, can promote cellular migration (*28*). While MuSCs can undergo migration in isolated myofibers in vitro (*29*), previous attempts to assess migration in vivo found that MuSCs do not migrate within an approximately 6-hour time frame (*16*). However, it remains unclear whether quiescent MuSCs in uninjured muscles are able to migrate over a longer time period. To assess their migratory behavior, we directly monitored MuSCs in a spatiotemporal manner within anesthetized Pax7EGFP animals (fig. S3A). A major challenge of imaging deep skeletal muscle of the lower leg is that it requires a skin incision to expose the deeper tissue layers, leading to both inflammatory and wound-healing responses (*30*). In contrast, the ear muscle is anatomically very close to the skin and provides a technical imaging advantage, as there is no need for a skin incision (fig. S3, B and C), thereby avoiding tissue disturbances or wound-induced chemoattractant signals (*31*) that could influence cell mobilization in the underlying muscle. Moreover, the intact skin has an anatomically characteristic pattern of hair follicles that can be used for orientation during imaging studies (*32*). By using the clusters of hair follicles as a landmark (fig. S3, D and E), we were able to pinpoint the exact region of interest in muscles and image it at different time points (fig. S3, F and G). This unique imaging method revealed that quiescent MuSCs remain in a relatively fixed position on the fibers under steady-state conditions over an 8-day duration (fig. S3, F and G). As the protrusion length in the majority of these quiescent adult MuSCs remains unaltered during this time period, we conclude that, in uninjured muscle fibers, protrusions do not promote MuSC migration.

MuSC protrusions are dynamically regulated upon skeletal muscle injury

Following injury, normally quiescent MuSCs are activated, proliferate, and either self-renew or differentiate, fuse, and ultimately reconstitute skeletal muscles (*33*). Because MuSCs play a pivotal role during muscle regeneration, we next sought to explore whether the MuSC subtypes we identified have distinct responses after injury. To this end, we induced muscle injury in the TA of Pax7EGFP mice with notexin and imaged their muscles at different times after injury (Fig. 2A). Analysis of MuSCs within the injury area (fig. S4A, white line) revealed that, after muscle damage, MuSC protrusions are reduced in length and that the MuSC population phenotype shifts toward cells with less protrusions at day 2 (d2) (Fig. 2C) and even more pronounced by d3 (Fig. 2D), a time point when proliferation peaks after injury (*34*), and results in a population of MuSCs that have predominantly zero to two, with very few remaining cells with more than 3. Analysis of muscle areas adjacent to the injury (fig. S4A, yellow line) revealed a similar shift of MuSC types toward cells with fewer protrusions (fig. S4B), suggesting that MuSC protrusions are dynamic and readjust their length in response to injury even from a distance. To gain insight into the cell cycle dynamics of MuSC subtypes within the injury, we used the Ki67–red fluorescent protein (RFP) line, which has been previously used to visualize actively proliferating cells in vivo (*35*). We first bred Ki67-RFP with Pax7EGFP mice to generate double Pax7EGFP/Ki67-RFP mice and then imaged their muscles at d3 after injury (fig. S5, A and B). Our analysis showed that predominantly cells with few protrusions are proliferative (fig. S5C), further indicating that cells with more protrusions represent putative quiescent stem cells, while cells with few protrusions are the more “active” MuSC population. Together, these data demonstrate that there is a distinct function of the different MuSC types, with cells with few protrusions primed to be the “first line” responders that are ready to proliferate immediately following injury. Coupled with data shown above,

these results indicate that cells with few protrusions are initially dormant, and they become activated later during the regeneration process, shifting toward a morphological cell state with less protrusions.

Fig. 2. MuSC protrusions are dynamically regulated during muscle regeneration.

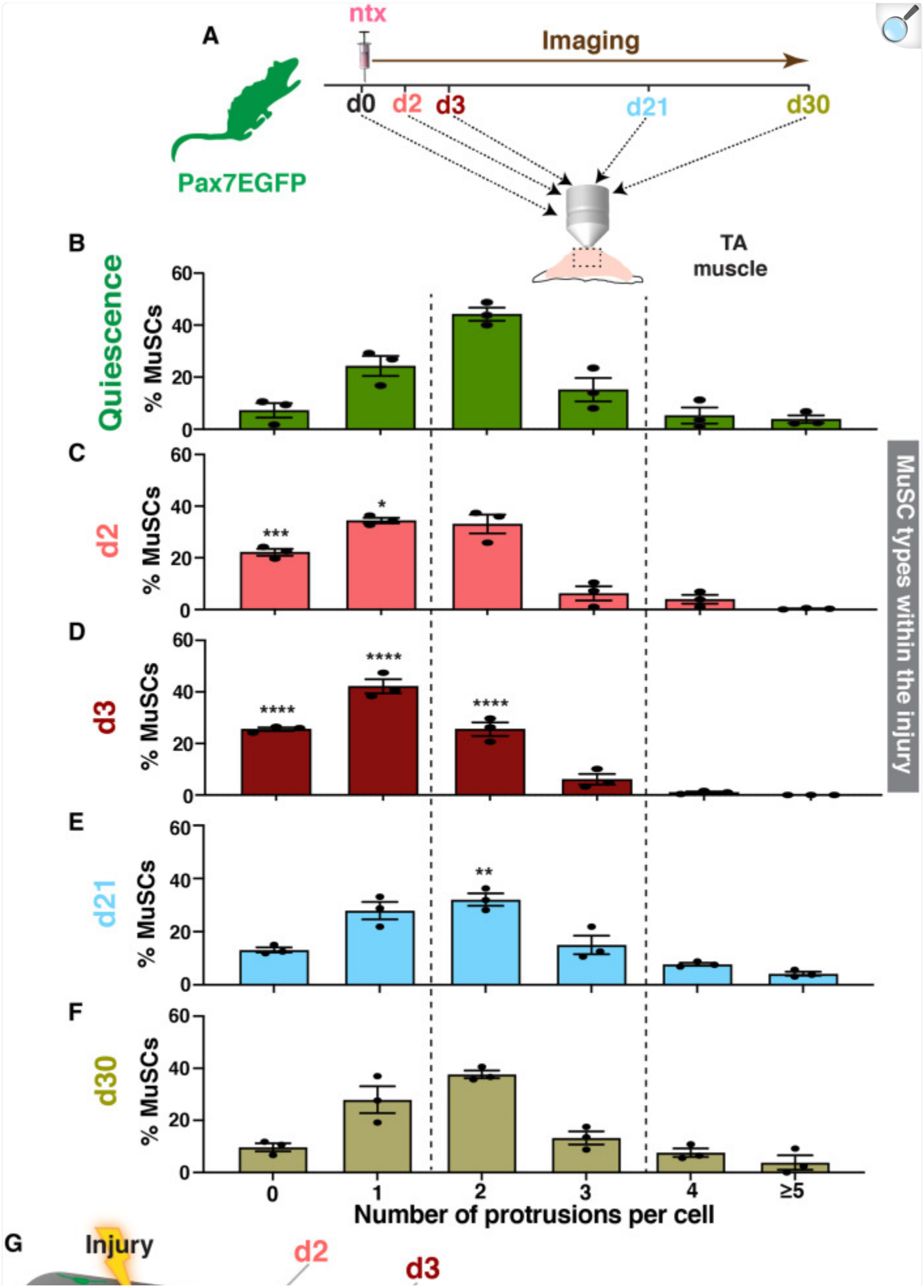
A
ntx
Imaging
d0
d2
d3
d21
d30
Pax7EGFP
TA muscle
B
Quiescence
C
d2
D
d3
E
d21
F
d30
% MuSCs
0
20
40
60
*
***
****
**
0
1
2
3
4
≥5
Number of protrusions per cell
MuSC types within the injury
G
Injury
d2
d3

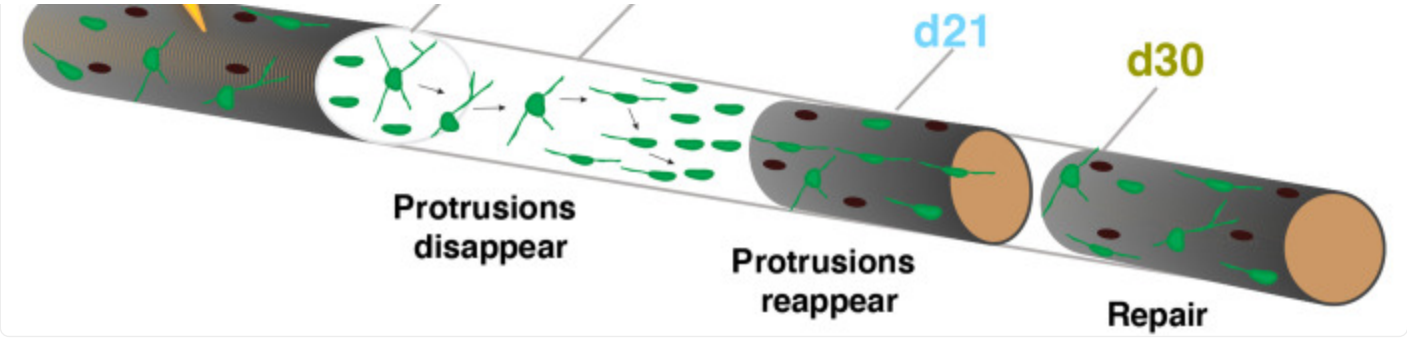

Open in a new tab

(**A**) Schematic representation of imaging the TA muscle at different time points (days) after notexin injury using two-photon microscopy. (**B**) Distribution of different MuSC types before injury. (**C**) Distribution of different MuSC types 2 days (d2) after injury shows a shift toward cells with less protrusions. (**D**) Distribution of MuSC types 3 days (d3) after injury. Note the disappearance of cells with multiple protrusions and the increase shift toward more cells with fewer protrusions. (**E**) Twenty-one days (d21) after injury, there is a redistribution of MuSC types, suggesting that protrusions reappear at later stages of regeneration. (**F**) At day 30 (d30), the distribution of MuSC types has returned to preinjury conditions. (**G**) Proposed model of the behavior of MuSCs during regeneration. There is a dynamic retraction of MuSC protrusions, with cells with few protrusions being the adaptive subtype that predominantly respond first, while cells with multiple protrusions are more dormant, and they reduce their protrusion length at a later phase. As tissue healing continues at later stages of regeneration, cellular protrusions reappear and cells align across the injured fiber, contributing to muscle repair and restoring the homeostatic MuSC morphological heterogeneity upon stem cell self-renewal. $n = 3$ mice (2 months old) were analyzed, and $N > 150$ cells per animal for each time point in (B) to (F). Data were analyzed by two-way ANOVA followed by Tukey's multiple comparisons test. Data from each day after injury (C to F) were compared with the equivalent data from the quiescence state (B). Values are presented as means ± SEM. *$P < 0.05$, **$P < 0.01$, ***$P < 0.001$, and ****$P < 0.0001$.

As regeneration proceeds, MuSCs down-regulate Pax7, and either differentiate or self-renew and reexpress Pax7 (*33*, *36*). By d21 after injury and as tissue restoration progresses, $EGFP^+$ cells again exhibit a wide range of MuSC states, including cells with more protrusions (Fig. 2E), showing that protrusions reappear in self-renewing MuSCs of regenerated myofibers. By d30, the distribution of the different MuSCs types returned to that found in preinjured muscles (Fig. 2, F and B). These data demonstrate that the dynamic regulation of MuSC protrusions concurs with the transitions between different functional phases during skeletal muscle regeneration (Fig. 2G). Collectively, our analyses demonstrate a dynamic retraction of MuSC protrusions in regenerating muscle fibers, with cells with few protrusions predominantly responding first, while cells with more protrusions reduce their protrusion length progressively and get activated at a later phase. As tissue healing continues and stem cell self-renewal occurs at later stages of regeneration, cellular protrusions reappear and restore homeostatic MuSC morphological heterogeneity, after a single or after repeated injuries (fig. S4C). Thus, our data indicate that MuSC protrusions are not static structures but instead adapt to distinct

regeneration phases, further supporting a coordinating role in muscle restoration.

Cell protrusions in G_{Alert} MuSCs adjust to a transitional state

It was previously shown that systemic signals can influence MuSCs to adapt to a "primed" or G_{Alert} state that enables them to quickly increase functional ability (*37*). On the basis of the morphological changes of MuSCs in response to injury, we hypothesized that MuSC protrusions are also regulated in G_{Alert} cells. To test this hypothesis, we injured one leg of Pax7EGFP mice with notexin and imaged the contralateral uninjured TA muscle (fig. S6A). MuSCs at the distal site show a shift toward cells with few protrusions (fig. S6B), analogous to that observed in MuSCs adjacent to the injury (fig. S4B). These findings further demonstrate that damage increases the proportion of MuSCs with few protrusions even at sites distal to the injured areas, consistent with the notion that these cells are more "adaptive" cells. While the total number of cells per muscle volume, the number of branches, and the orientation of the G_{Alert} cells remain unchanged (fig. S6, C to E), there is a notable reduction in the overall protrusion length (fig. S6F) and a shift toward a less elongated shape in the G_{Alert} cells compared to quiescent cells (fig. S6G). These findings further suggest that reduction in protrusion length promotes a more circular shape, in accordance with the fact that G_{Alert} cells are in an adaptive state ready to respond rapidly to a subsequent injury (*37*). Together, these data reveal that MuSC protrusions are delicate structures that respond to various levels and degrees of damage. Even after systemic injuries, MuSCs respond by shifting to a transitional, primed state characterized by an increased distribution of cells with few protrusions, further supporting our previous injury data (Fig. 2) that cells with zero to one protrusions are cells prepped to attain an active state.

MuSCs can be classified into responsive, intermediate, and sensory cells

On the basis of the various morphological and functional characteristics of the protrusions analyzed, we classified quiescent MuSCs into three different subtypes (table S1): (i) "Responsive" cells are smaller and rounder, with zero or one protrusion, that are aligned along the fiber. These are the primed, more active cells and the first ones to respond to an injury. (ii) "Sensory" cells, which are larger, less round cells that are not aligned along the fiber and have four or more protrusions, extended in all directions of the fiber and are more "dormant" cells that respond to injury at a later phase. (iii) "Intermediate" cells, which display intermediate sizes, are usually elongated, are not always aligned along the fiber and have two or three protrusions, and seem to be in between the above states. On the basis of our data, upon injury, sensory cells respond later, by losing their protrusions and transitioning toward intermediate and then responsive cells. This categorization of MuSCs' properties establishes a more defined context to investigate sensing pathways that could affect the transition from one state to another in response to injury.

Piezo1 regulates the morphological heterogeneity of MuSCs and is required for proper transition of MuSC subtypes during regeneration

Piezo1 is an emerging mechanosensing protein that acts as an important mediator of various aspects of mechanical signaling and cell fate regulation in osteoblasts (*27*) and axon regeneration (*38*). Although Piezo1 is expressed in MuSCs (*39*), its role in MuSC regulation has never been studied. To examine the effect of Piezo1 in MuSC morphological heterogeneity, we treated Pax7EGFP mice with a widely studied activator of Piezo1, called Yoda1 (Fig. 3A) (*40*). First, we confirmed that injection of Yoda1 does not affect the overall organ metrics (fig. S7, A to D). Next, we analyzed MuSC subtypes between uninjected Pax7EGFP mice and Pax7EGFP mice injected with dimethyl sulfoxide (DMSO) (fig. S7E) and found that DMSO alone has no effect on MuSC states. However, comparison of Pax7EGFP mice injected with either DMSO or Yoda1 revealed that while the total number of cells per volume remained unchanged (fig. S7F), MuSCs from Yoda1-injected mice shift to a primed state characterized by an increased distribution of responsive cells and a reduction of intermediate cells (Fig. 3B), had a reduced protrusion length (Fig. 3C), and were more circular in shape (Fig. 3D). These data demonstrate that pharmacological activation of Piezo1 shifts MuSCs toward a transitional activated state similar to G_{Alert} MuSCs (fig. S6), morphologically evident by the increased percentage of responsive cells, even in the absence of a regenerative signal.

Fig. 3. Pharmacological activation of Piezo1 primes responsive MuSCs.

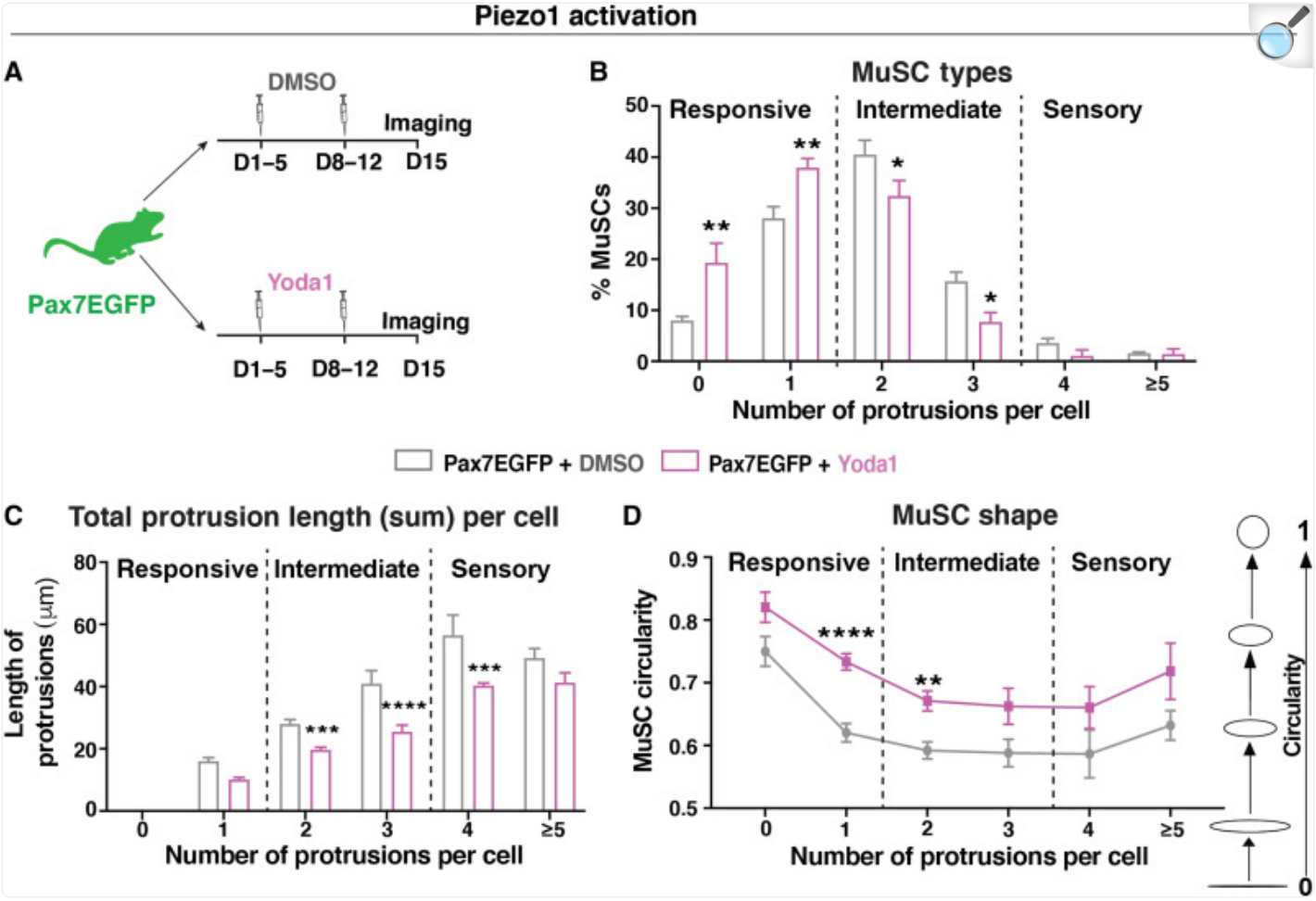

Open in a new tab

(**A**) Experimental scheme for pharmacological activation of Piezo via injection of Yoda1. Two-month-old male Pax7EGFP mice were injected with either DMSO or Yoda1 five consecutive days per week for 2 weeks (d1 to d5 and d8 to d12), and their TA was imaged at d15. (**B**) MuSCs from mice injected with Yoda1 show a shift toward more responsive cells. (**C**) Total protrusion length is decreased in MuSCs from mice injected with Yoda1. (**D**) MuSCs from mice injected with Yoda1 are less elongated. $n = 3$ to 4 mice (2 to 3 months old) were analyzed, and $N > 600$ cells per animal. Two-way ANOVA was used for analyses, followed by Šídák's multiple comparisons test. $*P < 0.05$, $**P < 0.01$, $***P < 0.001$, and $****P < 0.0001$.

To investigate whether Piezo1 is necessary and sufficient for the transition between functional MuSC subtypes, we generated mice in which Piezo1 is conditionally deleted in MuSCs. Specifically, mice carrying a floxed allele of Piezo1 (*41*) as well as the Ai9 allele (*42*) to track and image cells (tdTomato^{+}) were crossed with Pax7^{ERT2Cre} mice (*43*) to

generate Piezo1 MuSC-specific knockout (Piezo1$^{MuSC\text{-}KO}$) mice (fig. S8A). While ablation of Piezo1 in MuSCs had no effect on overall muscle morphology (fig. S8B) or total cell numbers per volume (fig. S8C) under steady-state conditions, the total length of MuSC protrusions was increased (Fig. 4A, fig. S8D, and movie S2) and cells were more elongated (Fig. 4B), consistent with an expansion of cell surface area that could potentially be used to explore their environment. Under uninjured conditions, quiescent and immotile MuSC populations were composed of significantly fewer responsive cells and more intermediate cells (Fig. 4C) with abnormal, spikey, and thick protrusions (Fig. 4D), indicative of alterations in the morphological shift of MuSCs. These data suggest that Piezo1 affects the morphological heterogeneity of cells at the progenitor level.

Fig. 4. MuSC-specific deletion of Piezo1 blocks transition of MuSCs toward responsive cells.

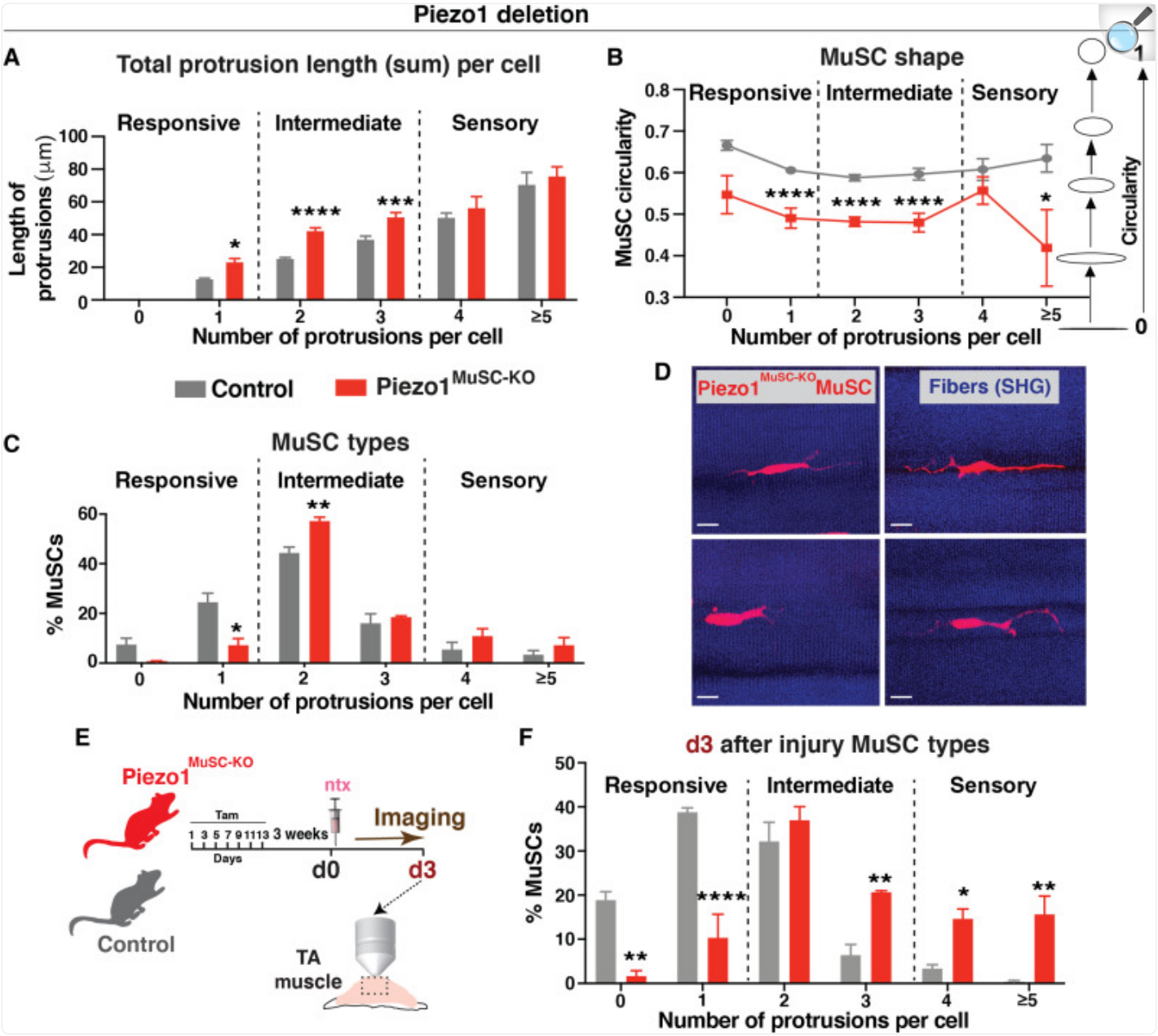

Open in a new tab

(**A**) Increased protrusion length in all types of Piezo1$^{MuSC\text{-}KO}$ MuSCs under steady-state conditions. (**B**) Cells are elongated in Piezo1$^{MuSC\text{-}KO}$ compared to control muscles under steady-state conditions. (**C**) Reduced number of responsive cells and increased number of sensory cells in Piezo1$^{MuSC\text{-}KO}$ muscles under steady-state conditions. (**D**) Representative images of Piezo1$^{MuSC\text{-}KO}$ MuSCs show the complexity of the protrusions in these cells. Scale bars, 10 µm. (**E**) Schematic representation of seven intraperitoneal tamoxifen (Tam)

injections and then notexin (ntx) injection 3 weeks after the last tamoxifen injection. Imaging of the TA muscle at d3 post-notexin injury using two-photon microscopy of control (gray) and Piezo1$^{MuSC\text{-}KO}$ (red) mice. (**F**) Significantly reduced number of responsive cells and excessive number of sensory cells (red columns) in Piezo1$^{MuSC\text{-}KO}$ muscles at d3 after injury, a time point that control muscles have negligible numbers of sensory cells (gray columns). $n = 3$ mice (3 months old) were analyzed, and $N > 600$ cells per animal. Two-way ANOVA was used for analyses, followed by Šídák's multiple comparisons test. $*P < 0.05$, $**P < 0.01$, $***P < 0.001$, and $****P < 0.0001$.

To examine whether the changes we observed in protrusion complexity, length, and MuSC subtypes can influence the regeneration potential of Piezo1$^{MuSC\text{-}KO}$ muscles, we performed intramuscular notexin injury on young control and Piezo1$^{MuSC\text{-}KO}$ mice (Fig. 4E) and imaged their muscles by two-photon microscopy. Consistent with our previous data (Fig. 2D), the majority of control MuSCs are predominantly responsive by d3, with very few sensory cells (Fig. 4F). In contrast, in Piezo1$^{MuSC\text{-}KO}$ muscles, there are significantly more sensory and intermediate cells and fewer responsive cells at d3 after injury (Fig. 4F), demonstrating a clear impairment of Piezo1$^{MuSC\text{-}KO}$ MuSCs to transition toward more active responsive cells upon injury. To address whether the defect in MuSC subtype regulation in Piezo1$^{MuSC\text{-}KO}$ MuSCs is caused by MuSC proliferation changes, we injured control and Piezo1$^{MuSC\text{-}KO}$ mice with notexin and pulsed in vivo with the nucleotide analog 5-ethynyl-2′-deoxyuridine (EdU) to label cells undergoing DNA replication (fig. S8E). While in uninjured muscles there were no proliferation differences, we observed significant reduction of the portion of MuSCs that were EdU^{+} in Piezo1$^{MuSC\text{-}KO}$ (fig. S8, F and G). These data demonstrate that the absence of Piezo1 in MuSCs leads to a lower rate of proliferation upon injury, which eventually contributes to an overall impairment of muscle regeneration over time (fig. S8H). Together, these data demonstrate that Piezo1 is sufficient to prime MuSCs toward more responsive, active cells and is necessary for the proper maintenance of the morphological heterogeneity of MuSC states and cell proliferation that tunes muscle homeostasis and regeneration.

Dystrophic muscles exhibit dysregulated MuSC subtypes, with lower Piezo1 levels and longer, more complex protrusions

In muscle diseases such as DMD, unrelenting, repetitive muscle damage elicits a constant need for regeneration (*44*). We and others have previously shown that although DMD is initiated by a structural genetic defect, it develops progressively into a stem cell disease due to improper MuSC activation (*12*, *45*). To allow for visualization of dystrophic MuSCs at the single-cell level, we crossed mdx mice carrying the dystrophin mutation (*46*) with the Pax7EGFP reporter mice (*17*). To determine the morphology of the protrusions in dystrophic MuSCs, we imaged whole muscles of young mdx/Pax7EGFP mice and found an increased number of EGFP^{+} cells with more complex appearance (Fig. 5A; fig. S9, A and B; and movie S3), mirroring the complexity of Piezo1$^{MuSC\text{-}KO}$ MuSCs. To investigate whether Piezo1 levels might be affected in dystrophic cells, we performed quantitative real-time polymerase chain reaction (qRT-PCR) in isolated MuSCs. Dystrophic MuSCs exhibit markedly reduced Piezo1 levels compared to controls (Fig. 5B), indicating

a severe defect of Piezo1 signaling in diseased MuSCs. Further analysis of the MuSC states revealed a significant decrease of responsive cells and an increase in sensory cells (Fig. 5C), suggesting a delay in the transition from sensory to intermediate to responsive cells, similar to what we observed in Piezo1$^{MuSC\text{-}KO}$ regenerating muscles. Furthermore, all dystrophic MuSC types have longer (Fig. 5, D and E), more branched, and thicker protrusions (fig. S9, D and E), indicative of a failure to properly regulate protrusions in chronic dystrophic conditions. As a result of the increased number and length of protrusions, dystrophic MuSCs also appear as more elongated (Fig. 5F) and slightly misoriented (fig. S9C) compared to quiescent MuSCs, similar to the expanded cell surface and elongated cells we observed in MuSCs from Piezo1$^{MuSC\text{-}KO}$ muscles. Together, these data demonstrate that the reduced levels of Piezo1 in diseased MuSCs coexist with an improper adjustment of protrusion length and fail to adequately regulate MuSC states in dystrophic muscles during repetitive injuries.

Fig. 5. Impaired regulation of MuSCs' protrusions and improper MuSC state distribution in muscular dystrophy.

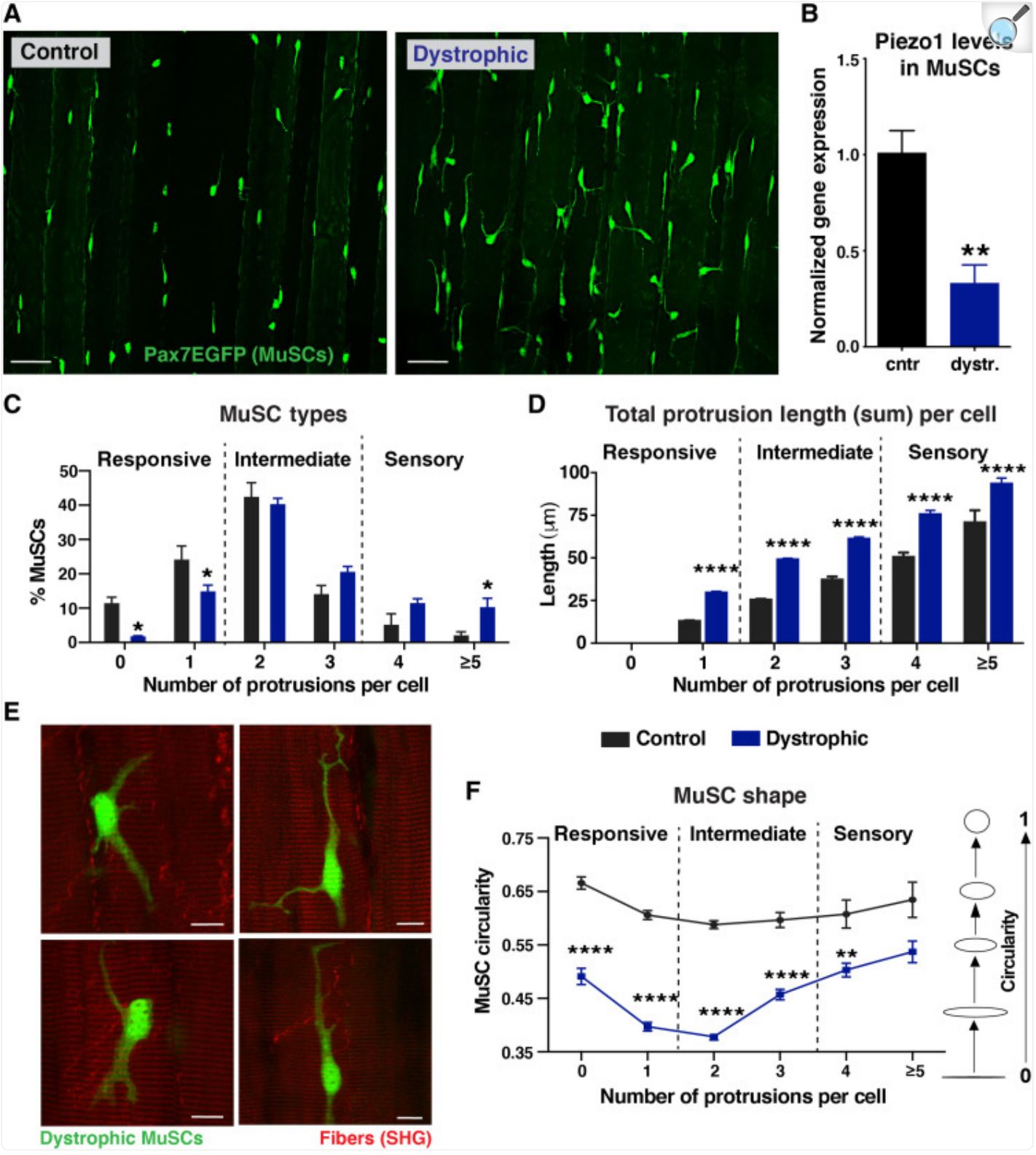

Open in a new tab

(**A**) Representative maximum intensity projections of an uninjured Pax7EGFP (left) and dystrophic (mdx/Pax7EGFP) muscle (right) at 3 months old. Note the increased number and complexity of protrusions in the dystrophic compared to uninjured muscles. Pax7EGFP MuSCs are shown in green. Scale bars, 50 μm. (**B**) qRT-PCR of *Piezo1* gene in control (cntr) (black) and dystrophic (dystr.) (blue) MuSCs shows down-regulation of *Piezo1* in dystrophic cells. $n = 3$ controls and $n = 6$ dystrophic animals (3 months old) for MuSC isolation. Results are shown as means ± SEM; statistical analysis was performed using unpaired Student's *t* test with Welch's correction, $^{**}P < 0.01$. (**C**) Reduced number of responsive cells and increased number of sensory cells in dystrophic muscles. (**D**) Increased protrusion length in all types of dystrophic MuSCs. (**E**) Representative images of dystrophic MuSCs show the complexity of the protrusions in these cells. Dystrophic cells are green (EGFP), and sarcomeres are marked by SHG in red. Scale bars, 10 μm. (**F**) Cells are significantly elongated in dystrophic compared to uninjured muscles. $n = 3$ to 4 mice (2 months old) were analyzed per condition, and $N > 400$ cells per mouse. Data in (C) to (E) were analyzed by two-way ANOVA, followed by Šídák's multiple comparisons test. Data in (B) were analyzed by unpaired *t* test with Welch's correction. Values are presented as means ± SEM. $^{*}P < 0.05$, $^{**}P < 0.01$, and $^{****}P < 0.0001$.

Activation of Piezo1 restores MuSC subtype distribution in dystrophic muscles

Because Piezo1 levels are reduced in dystrophic MuSCs, and MuSCs from Piezo1$^{MuSC\text{-}KO}$ and dystrophic mice display similar phenotypes (Figs. 4 and 5), we hypothesized that activation of Piezo1 pathway could alleviate the dystrophic MuSC morphology and function. To test this hypothesis, we used the known pharmacological activator of Piezo1, Yoda1 (*38*), which we previously demonstrated increases the percentage of responsive cells (Fig. 3B). mdx/Pax7EGFP mice were treated with either DMSO or Yoda1 (Fig. 6A), and their muscles were imaged by two-photon microscopy at d15 after treatment. First, we confirmed that DMSO alone had no effect on either the MuSC states (fig. S10A) or the complexity of the individual dystrophic MuSCs (fig. S10B). To determine the overall morphology of the protrusions, we imaged whole muscles of mdx/Pax7EGFP mice treated with either DMSO or Yoda1. We found that while the total number of EGFP^{+} cells remains unchanged (fig. S10D), the protrusions in the treated dystrophic muscles more closely resembled the morphology of a healthy muscle (Fig. 6B, fig. S10C, and movies S4 and S5). Analysis of MuSC states revealed a significant increase in responsive cells (Fig. 6C), suggesting a restoration in the transition from sensory to intermediate to responsive cells. Moreover, all MuSC types have shorter (Fig. 6D) and less complex protrusions (Fig. 6E) with reduced branches (fig. S10E), indicative of restoration of proper regulation of protrusions in chronic dystrophic conditions. As a result of the decreased number and length of protrusions, dystrophic MuSCs from Yoda1-treated animals also appear as less elongated (Fig. 6F) compared to dystrophic MuSCs from DMSO-treated dystrophic mice. When we examined the muscle cross sections of treated mice, we found evidence of improved regeneration in the Yoda1-treated dystrophic muscles, as shown by the increased fiber size as well as the number of fibers with centralized nuclei (fig. S10, F and G). Together, these data demonstrate that reactivation of Piezo1 in dystrophic muscles restores protrusion length, better regulates MuSC heterogeneity, and promotes proper function during repetitive injuries (fig.

S10H).

Fig. 6. Amelioration of dystrophic MuSC morphological defects after pharmacological activation of Piezo1.

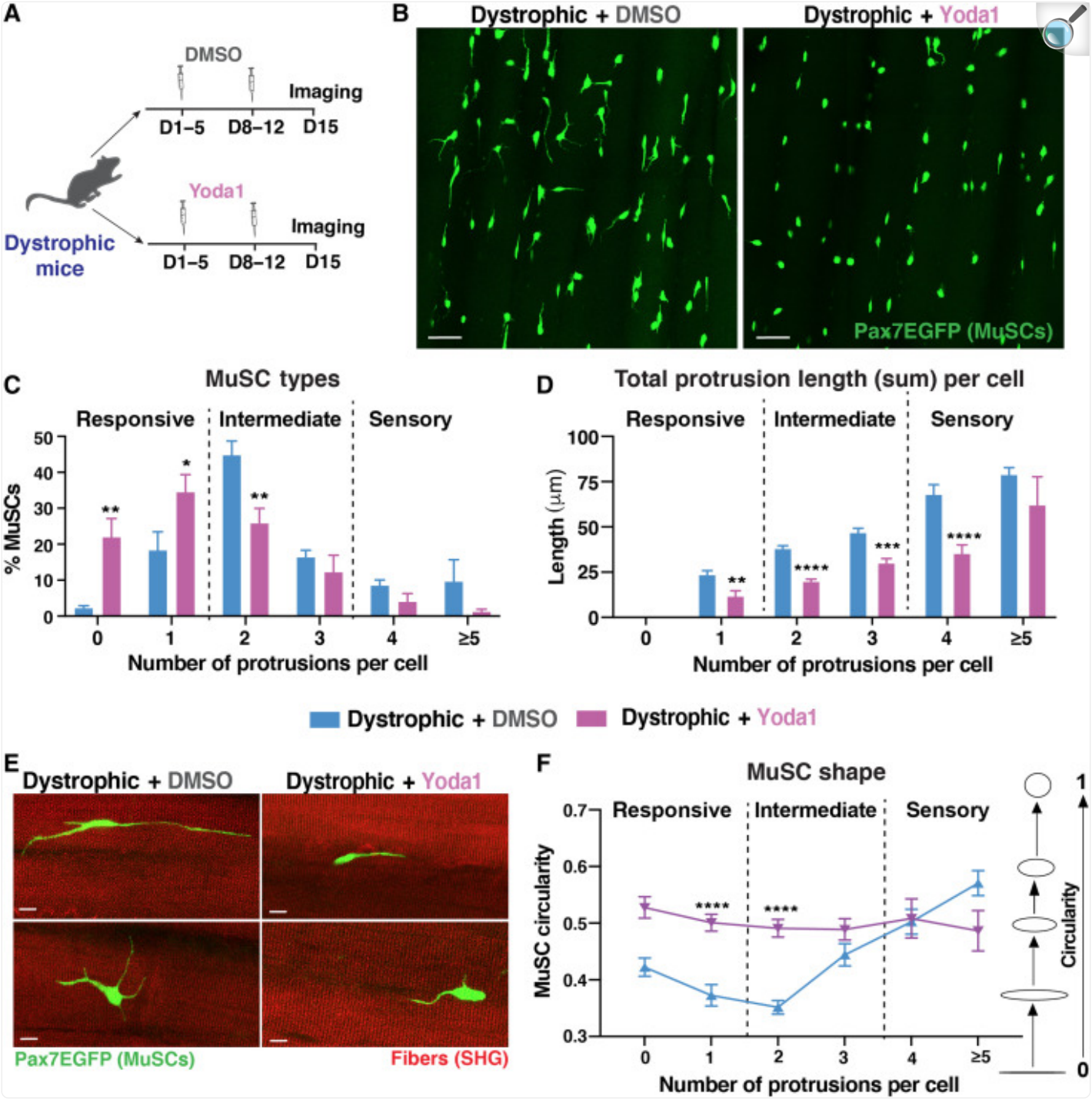

Open in a new tab

(**A**) Experimental scheme for pharmacological activation of Piezo1 in dystrophic mice. Two-month-old male mdx/Pax7EGFP mice were injected with either DMSO or Yoda1 for five consecutive days per week for 2

weeks (d1 to d5 and d8 to d12), and their TA was imaged at d15. (**B**) Representative maximum intensity projections of mdx/Pax7EGFP treated with DMSO (left) and dystrophic (mdx/Pax7EGFP) muscle treated with Yoda1 (right) at 2 months old. Note the reduced complexity of protrusions in the Yoda1-treated compared to the DMSO-treated muscles. Dystrophic MuSCs are shown in green. Scale bars, 60 μm. (**C**) Shift toward more responsive cells in Yoda1-treated dystrophic muscles compared to DMSO-treated muscles. (**D**) Protrusion length was brought down in all types of dystrophic MuSCs treated with Yoda1. (**E**) Representative images of dystrophic MuSCs from muscles treated with Yoda1 show the diminished complexity of the protrusions in these cells. Dystrophic cells are green (EGFP), and sarcomeres are marked by SHG in red. Scale bars, 10 μm. (**F**) Cells with zero to two protrusions in dystrophic muscles treated with Yoda1 are less elongated, better resembling the MuSC shape of a physiological muscle. $n = 4$ to 5 mice (2 months old) were analyzed per condition, and $N > 600$ cells per mouse. Data in (C), (D), and (F) were analyzed by two-way ANOVA, followed by Šídák's multiple comparisons test. Values are presented as means ± SEM. $*P < 0.05$, $**P < 0.01$, $***P < 0.001$, and $****P < 0.0001$.

DISCUSSION

MuSCs are essential for muscle homeostasis and regeneration, but their morphological and functional characterization has primarily been carried out through histological and single-fiber isolation analysis. Here, using a dynamic mouse line to follow stemness (*17*), we visualized quiescent MuSCs in their natural muscle environment by two-photon microscopy and found that MuSCs are morphologically heterogeneous, exhibiting a variety of axon-like protrusions. The majority of MuSCs display two protrusions, followed by cells with three and one protrusions, respectively. The lack of visible protrusions in isolated MuSCs suggests that they are very fragile and sensitive to environmental cues, consistent with previous observations (*15*) as well as with stem cell extensions in other organisms, which are visible only in vivo (*47*). One of the most well-characterized cellular extensions present on stem cells in many systems, including muscles, is the primary cilium, a single very short unbranched extension (*48*). However, the protrusions described here for adult MuSCs are long extensions that vary in both number and length, and a significant portion of MuSCs in adult uninjured muscles have branched protrusions, suggesting that protrusions and cilia are likely to be two distinct structures.

On the basis of the morphology and behavior of the protrusions, we classified adult quiescent MuSCs into three categories with distinct morphological and functional properties: responsive, intermediate, and sensory cells. We found that responsive cells are round and more primed, with zero or one protrusion; sensory cells are larger cells, in a more genuine, stem cell–like state and have four or more longer protrusions that extend in all directions of the fiber; and intermediate cells have two or three protrusions and are in between the other two states. Although some indications of cellular extensions were previously introduced (*15*, *49*, *50*), the extensive and full-range characterization of the MuSC protrusions in uninjured and regenerating muscles we report here has never been performed before. While cellular protrusions have been described in stem cells of other organisms and in other mammalian tissues (*15*, *47*, *51*–*53*), there

is little information regarding the exact function of such extensions in adult stem cells in this emerging field (*2*). Because of the loss of these fragile extensions upon isolation, conventional transplantation experiments or transcriptomic analysis in isolated cells cannot be used to gain insights into the molecular pathways and/or function of morphological distinct MuSC states.

To further investigate whether changes in the protrusions correlate with altered MuSC function and to determine whether MuSC protrusions may contribute to skeletal muscle healing, we studied their behavior under injury conditions. We found that newly characterized primed cells with fewer protrusions, we designated as responsive cells, are the first MuSC type to respond and participate in regeneration, followed by the transformation of cells in a more genuine stem cell state with more protrusions, we designated as sensory cells. These alterations occur following both local and systemic injury, further demonstrating that MuSCs undergo a timely adaptive response following injury. It has been reported that MuSCs with higher Pax7 levels are less primed for myogenic commitment at the transcription level and take longer to enter the cell cycle (*36*). Our study provides evidence that sensory cells (with more protrusions) respond to injury later than responsive MuSCs (with fewer protrusions), presumably because it takes them longer to transition toward intermediate and responsive cells. The dynamic transition of MuSCs during early activation is consistent with a previous report showing changes in mechanoproperties and cytoskeleton signaling before cell cycle signaling (*3*). The differential timing of responsive and sensory cells during regeneration that we observe is consistent with the notion that not all quiescent MuSCs are functionally equivalent, with responsive cells (fewer protrusions) being more primed cells, as shown both in the injury and their response in the G_{Alert} phase, while sensory cells (more and longer protrusions) are more dormant and intermediate cells are in between these states. These data suggest a hierarchical cascading quiescence model, in which the responsive cells facilitate a rapid response to injury, while sensory cells only participate in high-demand injury situations, where they lose protrusions and transition toward intermediate and responsive cells. Overall, contrary to the idea that quiescence is simply a passive and dormant state, our results reveal that quiescent MuSC populations represent a collection of morphological heterogeneous states with different functional capabilities. These findings provide a detailed morphological heterogeneity in MuSCs in their endogenous environment and lay the groundwork for future spatial molecular analysis of the different MuSC states using methods recently developed for other tissues (*54*, *55*).

Adult stem cells often reside in specialized microenvironments, called niches, that specify stem cell identity (*56*). While we found that MuSC protrusions do not mobilize cells under steady-state conditions, we suspect that they may play an important role in sensing both the niche environment and the surrounding muscle. In support, at a later stage of regeneration where self-renewal occurs and MuSCs return to their niche to preserve progenitors for response to future injuries (*33*), the protrusions reappear, and the morphological heterogeneity is restored as in preinjured muscles. Consistent with the notion that protrusions are important to specify stemness and proper identity at the niche, lack of protrusions in isolated MuSCs are associated with a reported loss of stemness and rapid differentiation in vitro (*33*), which hinders MuSC stem cell maintenance in cultures. Protrusions act as an effective and specific form of cell communication in a variety of cell types (*2*). Our analysis showed that responsive MuSCs are in close proximity to other

nuclei on the myofibers. As such, the proximity between MuSC protrusions and endothelial cells could regulate stem cell quiescence via Notch signaling (*15*) or be used for communication with other progenitor cells within skeletal muscles, i.e., fibroadipogenic progenitors, which provide functional support to MuSCs (*57*). It is possible that disruption of such communication via improper regulation of MuSC protrusions could contribute to the incomplete regeneration seen in diseased muscles (*58*). Future investigation of additional intrinsic and extrinsic regulators or other sensors that could be responsible for preserving MuSC protrusions, in combination with extracellular matrices that mimic the living architectural muscle cues (*59*) and retain cell-matrix interactions, including nerve injuries that were recently shown to affect MuSC morphology (*60*), would allow direct assessment of the essential communication between MuSC states, the niche, and the surrounding environment, including the neuromuscular and myotendinous junctions.

Pharmacological approaches to interfere with the generation of cytoskeletal protrusions in vivo are unlikely to be tenable as skeletal muscle fibers consist of the same cytoskeletal molecules and will also be affected. Instead, here, we found a critical role for the sensing protein PIEZO1 in regulating the morphological heterogeneity of MuSCs using both mouse genetic and pharmacological approaches. Since its original identification (*41*), the importance of Piezo1 has been revealed in various tissues (*61*–*63*). Yet, there is only a limited understanding of how Piezo1 acts in stem cells and how it shapes biological processes [discussed in (*25*)]. The work presented here demonstrated that Piezo1 is essential for maintaining MuSC states and regulating protrusion length and cell shape in both homeostatic and dystrophic muscles. We show that pharmacological activation of Piezo1, via Yoda1, is sufficient to shift MuSCs to a transitional, primed state that is characterized by an increased distribution of responsive cells and promotes an adaptive, more active MuSC state. Although detecting expression levels in whole muscles while preserving the morphological heterogeneity of MuSCs is still a challenge, we postulate that Piezo1 may be expressed at very low basal levels in sensory cells, which have long protrusions extending along and across the fiber, allowing them to sense the surrounding environment. However, upon ablation of Piezo1 in MuSCs, there is a clear shift in distribution toward fewer responsive cells that becomes more profound at d3 after injury, whereas the number of sensory cells is significantly increased and disproportional compared to d3 control MuSC states. These data further suggest that in the absence of Piezo1, MuSCs lengthen their protrusions to better perceive their injured immediate microenvironment and reduce their proliferation rate at the cost of delaying muscle regeneration, in agreement with previous reports (*64*, *65*) and consistent with the idea that inactivation of proper cell channels impedes a transition from a resting state to an activated state (*3*, *25*, *27*).

The importance of Piezo1 in muscle disease is further displayed by studying young dystrophic muscles in their endogenous environment. We propose that although dystrophic MuSCs perceive muscle damage, they do not properly "sense" it due to their lower Piezo1 levels. As a result, they expand their protrusions and elongate their shape to counterbalance this inability to transmit information. An alternative hypothesis might be that Piezo1 provides a feedback signal that "informs" these cells when they have stretched enough. In this case, a reduced feedback signal due to the lower levels of Piezo1 would lead to elongation and protrusion expansion. Either way, we suggest that under the high regenerative demands in the diseased muscles, dystrophic cells are unable to channel the information in a timely manner, leading to the reported improper MuSC activation in dystrophic muscles (*12*). To test this assertion, we next

asked whether temporary pharmacological activation of Piezo1 was sufficient to reverse the defective morphology of dystrophic MuSCs. Our data revealed that administration of Yoda1 restores MuSC state distribution, shortens protrusion length, and alters stem cell shape to more closely resemble a healthy MuSC, while muscle regeneration is boosted. The duration of the effects of such a treatment on MuSCs and whether additional boosts or different doses might be necessary to maintain MuSC morphology and function in dystrophic muscles over a longer period of time remain to be tested. Moreover, Piezo1 is a bona fide mechanosensitive channel that mediates Ca^{2+} signaling in various cell types (*25*–*27*, *39*, *60*, *65*). Thus, we cannot exclude that microenvironmental changes in other muscle cells and/or myofibers may also influence MuSC function and morphology. Nevertheless, the data presented here provide proof of principle of the therapeutic potential of Yoda1 in restoring MuSC heterogeneity in dystrophic muscles.

In summary, we demonstrated a unique morphological heterogeneity of adult MuSCs and revealed that regulation of MuSC subtypes and protrusion length play a fundamental role in skeletal muscles in health and disease. This work constitutes a pioneering step in defining new structural and behavioral properties of MuSC progenitors and demonstrates that the underlying molecular mechanism involving the sensing pathway Piezo1 is critical for preserving a healthy morphological heterogeneity of the stem cell pool and maintaining the regeneration potential of skeletal muscles. Our study provides essential and fresh insights for addressing crucial questions regarding the biology and communication of stem cells with their environment in physiological and pathological conditions and presents a therapeutic target for treating muscular dystrophy. Given the emerging interest of protrusions on stem cells in other systems (*47*, *53*, *66*), the findings and molecular mechanism presented here for MuSCs are likely to be relevant for other adult stem cell populations with cellular extensions in different tissues and organisms.

MATERIALS AND METHODS

Animals

Adult Pax7EGFP (*17*) mice were bred with either mdx^{4cv} mice (The Jackson Laboratory, stock no. 002378) to generate double mdx^{4cv}; Pax7EGFP or RosanTnG mice (The Jackson Laboratory, stock no. 023035) to generate double Pax7EGFP; nTnG mice. Ki67-RFP mice (The Jackson Laboratory, stock no. 029802) were bred with the Pax7EGFP mice to generate the double Pax7EGFP;Ki67-RFP mice (fig. S4A). $Piezo1^{Fl/Fl}$ mice (The Jackson Laboratory, stock no. 029213) were crossed to $Ai9^{Fl/Fl}$ mice (The Jackson Laboratory, stock no. 007909) and Pax7ERT2Cre mice (The Jackson Laboratory, stock no. 017763) to create the triple Pax7ERT2Cre;$Piezo1^{Fl/Fl}$;$Ai9^{Fl/Fl}$ mice (called $Piezo1^{MuSC\text{-}KO}$). To induce Cre expression, mice were injected with 250 μl of tamoxifen (Sigma-Aldrich; 20 mg/ml in ethanol/corn oil in a 1:10 ratio) intraperitoneally every second day for a total of seven injections, starting at 6 or 8 weeks of age. Genotyping was performed by PCR as described in (*17*). For all experiments, mice of the same sex and similar age were compared. The age of mice for each experiment is reported in the figure legends. Animals were housed and bred in a local animal facility at a 12-hour dark/12-hour light cycle, and their use and care were approved by the University of Pennsylvania according to Institutional Animal Care and Use Committee guidelines.

Muscle injury

To define MuSC number and protrusion status, the TA muscles of Pax7EGFP and genetically modified mice bred to Pax7EGFP mice were injured with notexin (10 μg/ml; Latoxan) at the ages indicated in each experiment. In the case of multiple injuries, a second injection of notexin was performed 1 week after the first injury and muscles were analyzed 10 days after the last injury. For G_{Alert} MuSCs, the TA of one hindlimb was injured once with 10 μl of notexin, and 3 days after injury, the TA muscle of the contralateral leg was analyzed as described below (see the "Image analyses" section).

Yoda1 injections

Yoda1 (Tocris Bioscience) was dissolved in DMSO at 40 mM as stock, diluted in 5% ethanol, and injected at 5 μmol/kg of body weight. Control mice were injected with equal volume of vehicle (DMSO diluted in 5% ethanol). Yoda1 or vehicle was injected intraperitoneally for five consecutive days per week for 2 weeks (d1 to d5 and d8 to d12). At d5, mice were harvested, and tissues were collected for further evaluation. All investigators involved in data collection were blinded to both genotype and group of mice.

Method details

Muscle isolation

Mice were euthanized by CO_2 asphyxiation, followed by cervical dislocation. The TA muscles were freshly dissected. Samples were then fixed in 4% paraformaldehyde (PFA)/1× phosphate-buffered saline (PBS) for 2 hours on a rocker mixer at 4°C and rinsed and stored in 1× PBS solution at 4°C in the dark.

Muscle histology

Muscles were dissected and fixed in 4% PFA/PBS and incubated overnight in 30% sucrose before being embedded in optimal cutting temperature embedding compound (Tissue-Tek; Sakura Finetek USA) and frozen in chilled 2-methylbutane. Cryosections were cut at a thickness of 10 μm. Sections were stained with hematoxylin and eosin and/or trichrome staining using standard procedures.

Immunofluorescence staining

Tissue cryosections were permeabilized in 0.5% Triton X-100/PBS for 10 min, washed with PBS, and incubated with

blocking solution [1% bovine serum albumin (BSA)/PBS/0.1% Triton X-100] for 1 hour at room temperature. Primary antibody for laminin (1:200; anti–laminin B2, clone A5, EMD Millipore Corp.) was incubated overnight at 4°C in antibody dilution buffer (1% BSA/PBS/0.1% Triton X-100). Slides were then incubated with secondary antibody [Alexa Fluor 647-conjugated goat anti-rat (1:300; Thermo Fisher Scientific)] in antibody dilution buffer for 1 hour in the dark. Slides washed with PBS, and coverslips were mounted with ProLong Gold with 4′,6-diamidino-2-phenylindole (DAPI) (Thermo Fisher Scientific). Sections were imaged with a Nikon Ni wide-field epifluorescence microscope equipped with a 20× Plan Apo objective and Nikon Elements software.

Two-photon microscopy

Fixed muscles were mounted on a custom-made glass chamber and immersed in 1× PBS, and a coverslip was lowered from the top to close the chamber. High-resolution serial optical sections were collected from the top of the muscle after the collagen deposition layer, using a Leica SP* Confocal/Multiphoton Microscope system equipped with a Chameleon Vision II Sapphire laser. A 910-nm laser was focused through a 20× HCX APO L Lens. The following acquisition settings were used for the collection channels: High Voltage (HV): 550/525 V, gain: 1/1, offset: 3/4%. Emission light was collected with a fluorescein isothiocyanate [Bandpass (BP) 525/50] filter, and muscle fibers were marked via SHG in blue channel. Serial optical sections were collected in 1.5-μm steps for a total range of 100- to 200-μm depth, flattened, and normalized to the volume scanned. For imaging of live animals, mice were anesthetized using a ketamine/xylazine mixture [ketamine (100 mg/kg) and xylazine (10 mg/kg)], administrated by intraperitoneal injection, and the skin in the ear and head was depilated. The mouse was placed on a heated stage, and the head and the ear were supported by a custom-made stage. A glass coverslip was placed against the skin in the junction region between the head and the ear. Distinctive inherent landmarks in the skin were used to navigate back to the original field of view and visualize the same follicles in separate experiments. Anesthesia was maintained throughout the course of the experiment with vaporized isoflurane delivered by a nose cone. The setup for in vivo microscopy was centered on an AxioTech-Vario 100 microscope (Olympus), equipped with light-emitting diode (LED) excitation light for fluorescence epi-illumination. Microscopic images were obtained with a water-dipping objective (20×, numerical aperture of 0.5) and acquired with an AxioCam HSm camera and AxioVision 4.6 software. Serial optical sections were acquired in 2-μm steps to image a total depth of ~150 μm of tissue.

Image analyses

Acquired optical sections from two-photon microscopy were analyzed in Fiji. To define MuSC number in the TA muscle, acquired optical sections were stacked in Fiji, and MuSCs were counted and normalized to the volume stacked. To quantify the length and number of the protrusions of MuSC, between 150 and 600 MuSCs per image were analyzed using the Simple Neurite Tracer (SNT) plugin in Fiji. MuSC circularity/aspect ratio, circularity, and orientation ratio were measured using set measurements and the angle tool in Fiji. N = number of cells analyzed per mouse can be found in the figure legends. At least two independent investigators blindly analyzed all data. Cells were defined as misaligned

with myofiber if the angle between the cell body and myofiber is greater than a 15-degree angle, and the ratio is calculated as the number of cells misaligned divided by the total number of cells per cell type.

MuSC isolation

Pax7EGFP mice were sacrificed, and the TA, quadriceps, and gastrocnemius muscles were dissected from both hindlimbs. Muscle was finely minced and placed in a C tube (Miltenyi) containing 0.15% collagenase in 10 ml of Dulbecco's modified Eagle's medium (DMEM). Tubes were loaded into MACS Dissociator (Miltenyi), and the manufacturer's muscle-01 program was run. Tubes were incubated at 37°C for 30 min, subjected to the muscle-01 program again, and incubated at 37°C for an additional 30 min. Seventy-five microliters of 2% collagenase (Sigma-Aldrich) and 75 μl of dispase (4.8 U/ml; Roche) were added, and tubes were vortexed at maximum speed before a 30-min incubation at 37°C. Cells were passed through a 21-gauge needle until all muscles were broken apart. The remaining cell slurry was filtered through a 40-μm cell strainer that was prewet with 10 ml of cold myoblast medium (DMEM:F12; 15% fetal bovine serum and 1× anti-anti), the strainer was rinsed with an additional 10 ml of cold myoblast medium, and cells were pelleted at 300*g* at 4°C. Cells were incubated with 1 ml of 1× red cell lysis buffer (Thermo Fisher Scientific) for 5 min at room temperature, and 9 ml of cold fluorescence-activated cell sorting (FACS) buffer [1% BSA, 2.5% goat serum, and 2 mM EDTA (pH 8.0) in 1× PBS] was added. Cells were spun, and cell pellets were resuspended in 1 ml of FACS buffer. Before FACS, 1 μg of the viability dye DAPI was added to each sample. Live GFP-positive MuSCs were isolated using an Aria II sorter equipped with a 100-μm nozzle. DAPI was excited with a 405-nm laser, and dead cells were identified using a 450/40 bandpass filter. GFP was excited with a 488-nm laser, and Pax7EGFP MuSCs were identified with a 530/30 bandpass filter.

Quantitative real-time polymerase chain reaction

RNA was isolated from FACS-sorted MuSCs using an RNeasy Plus Micro kit (Qiagen), according to the manufacturer's instructions. Complementary DNA (cDNA) was generated with the ProtoScript II First-Strand cDNA Synthesis Kit (New England Biolabs). qRT-PCR was carried out on a QuantStudio 6 instrument (Applied Biosystems) using TaqMan primers and TaqMan Universal PCR Master Mix. Reactions were carried out in quadruplicate. The number of animals used per experiment is indicated in the figure legends. Gene expression was determined using the $\Delta\Delta C_t$ method. Primers were purchased from Applied Biosystems and included Piezo1-FAM (Mm012415449_m1) and GAPDH-VIC (4352339e).

Quantification and statistical analyses

Values are presented as means ± SEM. n = number of mice per genotype. N = number of cells analyzed per mouse. Significance was determined using unpaired Student's t tests with Welch's correction or two-way analysis of variance

(ANOVA) using GraphPad Prism 7 software. Specific details on mouse numbers, age, and statistics can be found in the figure legends. All data were blindly analyzed by at least two independent investigators. *$P < 0.05$, **$P < 0.01$, ***$P < 0.001$, and ****$P < 0.0001$; n.s., not significant.

Acknowledgments

We thank the Hill Pavilion Animal Facility staff for assistance. Special thanks to G. Ruthel, technical director at the Penn Vet Imaging Core, for support and guidance with two-photon microscopy. We would like to thank J. Kim for help with tissue isolation as well as the undergraduate student G. Li for help with unbiased validation and data analysis assistance.

Funding: This study was supported by startup funds from Perelman School of Medicine, the NASA (80NSSC19K1602), and the NIH/National Institute of Arthritis and Musculoskeletal and Skin Diseases (R01HL146662) to F.M. Two-photon microscopy was supported by the NIH (S10 OD021633-01).

Author contributions: N.M. acquired two-photon images, performed experiments, and analyzed and interpreted data. D.C., J.-H.L., and E.B.H. organized the maintenance of the mouse colonies and performed and analyzed experiments. P.K. acquired two-photon images. J.K. assisted with the mouse colony and imaging analysis. H.H. and E.D.T. performed injections. P.R. supervised and performed imaging acquisition. F.M. conceived the original idea, designed and supervised all experiments, directed the project, interpreted data, and wrote the manuscript. All authors edited the manuscript.

Competing interests: The authors declare that they have no competing interests.

Data and materials availability: All data needed to evaluate the conclusions in the paper are present in the paper and/or the Supplementary Materials.

Supplementary Materials

This PDF file includes:

Figs. S1 to S10

Table S1

Click here for additional data file. (12.1MB, pdf)

Other Supplementary Material for this manuscript includes the following:

Movies S1 to S5

Click here for additional data file. (27.6MB, zip)

View/request a protocol for this paper from *Bio-protocol*.

REFERENCES AND NOTES

1. Heldin C. H., Lu B., Evans R., Gutkind J. S., Signals and receptors. Cold Spring Harb. Perspect. Biol. 8, a005900 (2016). [DOI] [PMC free article] [PubMed] [Google Scholar]

2. Buszczak M., Inaba M., Yamashita Y. M., Signaling by cellular protrusions: Keeping the conversation private. Trends Cell Biol. 26, 526–534 (2016). [DOI] [PMC free article] [PubMed] [Google Scholar]

3. Eliazer S., Muncie J. M., Christensen J., Sun X., D'Urso R. S., Weaver V. M., Brack A. S., Wnt4 from the niche controls the mechano-properties and quiescent state of muscle stem cells. Cell Stem Cell 25, 654–665.e4 (2019). [DOI] [PMC free article] [PubMed] [Google Scholar]

4. Engler A. J., Sen S., Sweeney H. L., Discher D. E., Matrix elasticity directs stem cell lineage specification. Cell 126, 677–689 (2006). [DOI] [PubMed] [Google Scholar]

5. Gilbert P. M., Havenstrite K. L., Magnusson K. E. G., Sacco A., Leonardi N. A., Kraft P., Nguyen N. K., Thrun S., Lutolf M. P., Blau H. M., Substrate elasticity regulates skeletal muscle stem cell self-renewal in culture. Science 329, 1078–1081 (2010). [DOI] [PMC free article] [PubMed] [Google Scholar]

6. Iskratsch T., Wolfenson H., Sheetz M. P., Appreciating force and shape-the rise of mechanotransduction in cell biology. Nat. Rev. Mol. Cell Biol. 15, 825–833 (2014). [DOI] [PMC free article] [PubMed] [Google Scholar]

7. Zammit P. S., All muscle satellite cells are equal, but are some more equal than others? J. Cell Sci. 121, 2975–2982 (2008). [DOI] [PubMed] [Google Scholar]

8. Relaix F., Bencze M., Borok M. J., der Vartanian A., Gattazzo F., Mademtzoglou D., Perez-Diaz S., Prola A., Reyes-Fernandez P. C., Rotini A., Taglietti V., Perspectives on skeletal muscle stem cells. Nat. Commun. 12, 692 (2021). [DOI] [PMC free article] [PubMed] [Google Scholar]

9. Mauro A., Satellite cell of skeletal muscle fibers. J. Biophys. Biochem. Cytol. 9, 493–495 (1961). [DOI] [PMC free article] [PubMed] [Google Scholar]

10. Brack A. S., Pax7 is back. Skelet. Muscle 4, 24 (2014). [DOI] [PMC free article] [PubMed] [Google Scholar]

11. Chang N. C., Chevalier F. P., Rudnicki M. A., Satellite cells in muscular dystrophy–Lost in polarity. Trends Mol. Med. 22, 479–496 (2016). [DOI] [PMC free article] [PubMed] [Google Scholar]

12. Sacco A., Mourkioti F., Tran R., Choi J., Llewellyn M., Kraft P., Shkreli M., Delp S., Pomerantz J. H., Artandi S. E., Blau H. M., Short telomeres and stem cell exhaustion model Duchenne muscular dystrophy in mdx/mTR mice. Cell 143, 1059–1071 (2010). [DOI] [PMC free article] [PubMed] [Google Scholar]

13. Tichy E. D., Sidibe D. K., Tierney M. T., Stec M. J., Sharifi-Sanjani M., Hosalkar H., Mubarak S., Johnson F. B., Sacco A., Mourkioti F., Single stem cell imaging and analysis reveals telomere length differences in diseased human and mouse skeletal muscles. Stem Cell Rep. 9, 1328–1341 (2017). [DOI] [PMC free article] [PubMed] [Google Scholar]

14. Tichy E. D., Ma N., Sidibe D., Loro E., Kocan J., Chen D. Z., Khurana T. S., Hasty P., Mourkioti F., Persistent NF-κB activation in muscle stem cells induces proliferation-independent telomere shortening. Cell Rep. 35, 109098 (2021). [DOI] [PMC free article] [PubMed] [Google Scholar]

15. Verma M., Asakura Y., Murakonda B. S. R., Pengo T., Latroche C., Chazaud B., McLoon L. K., Asakura A., Muscle satellite cell cross-talk with a vascular niche maintains quiescence via VEGF and notch signaling. Cell Stem Cell 23, 530–543.e9 (2018). [DOI] [PMC free article] [PubMed] [Google Scholar]

16. Webster M. T., Manor U., Lippincott-Schwartz J., Fan C. M., Intravital imaging reveals ghost fibers as architectural units guiding myogenic progenitors during regeneration. Cell Stem Cell 18, 243–252 (2016). [DOI] [PMC free article] [PubMed] [Google Scholar]

17. Tichy E. D., Sidibe D. K., Greer C. D., Oyster N. M., Rompolas P., Rosenthal N. A., Blau H. M., Mourkioti F., A robust Pax7EGFP mouse that enables the visualization of dynamic behaviors of muscle stem cells. Skelet. Muscle 8, 27 (2018). [DOI] [PMC free article] [PubMed] [Google Scholar]

18. Jockusch H., Voigt S., Migration of adult myogenic precursor cells as revealed by GFP/nLacZ labelling of mouse transplantation chimeras. J. Cell Sci. 116, 1611–1616 (2003). [DOI] [PubMed] [Google Scholar]

19. Gunther S., Kim J., Kostin S., Lepper C., Fan C.-M., Braun T., Myf5-positive satellite cells contribute to Pax7-dependent long-term maintenance of adult muscle stem cells. Cell Stem Cell 13, 590–601 (2013). [DOI] [PMC free article] [PubMed] [Google Scholar]

20. Pisconti A., Cornelison D. D., Olguin H. C., Antwine T. L., Olwin B. B., Syndecan-3 and Notch cooperate in regulating adult myogenesis. J. Cell Biol. 190, 427–441 (2010). [DOI] [PMC free article] [PubMed] [Google Scholar]

21. Bentzinger C. F., von Maltzahn J., Dumont N. A., Stark D. A., Wang Y. X., Nhan K., Frenette J., Cornelison D. D. W., Rudnicki M. A., Wnt7a stimulates myogenic stem cell motility and engraftment resulting in improved muscle strength. J. Cell Biol. 205, 97–111 (2014). [DOI] [PMC free article] [PubMed] [Google Scholar]

22. Morgan J. E., Partridge T. A., Muscle satellite cells. Int. J. Biochem. Cell Biol. 35, 1151–1156 (2003). [DOI] [PubMed] [Google Scholar]

23. Collins C. A., Zammit P. S., Isolation and grafting of single muscle fibres. Methods Mol. Biol. 482, 319–330 (2009). [DOI] [PubMed] [Google Scholar]

24. Behrndt M., Salbreux G., Campinho P., Hauschild R., Oswald F., Roensch J., Grill S. W., Heisenberg C. P., Forces driving epithelial spreading in zebrafish gastrulation. Science 338, 257–260 (2012). [DOI] [PubMed] [Google Scholar]

25. Nourse J. L., Pathak M. M., How cells channel their stress: Interplay between Piezo1 and the cytoskeleton. Semin. Cell Dev. Biol. 71, 3–12 (2017). [DOI] [PMC free article] [PubMed] [Google Scholar]

26. Sugimoto A., Miyazaki A., Kawarabayashi K., Shono M., Akazawa Y., Hasegawa T., Ueda-Yamaguchi K., Kitamura T., Yoshizaki K., Fukumoto S., Iwamoto T., Piezo type mechanosensitive ion channel component 1 functions as a regulator of the cell fate determination of mesenchymal stem cells. Sci. Rep. 7, 17696 (2017). [DOI] [PMC free article] [PubMed] [Google Scholar]

27. Wang L., You X., Lotinun S., Zhang L., Wu N., Zou W., Mechanical sensing protein PIEZO1 regulates bone homeostasis via osteoblast-osteoclast crosstalk. Nat. Commun. 11, 282 (2020). [DOI] [PMC free article] [PubMed] [Google Scholar]

28. Yang D., Qu F., Cai H., Chuang C. H., Lim J. S., Jahchan N., Grüner B. M., S Kuo C., Kong C., Oudin M. J., Winslow M. M., Sage J., Axon-like protrusions promote small cell lung cancer migration and metastasis. eLife 8, (2019). [DOI] [PMC free article] [PubMed] [Google Scholar]

29. Siegel A. L., Atchison K., Fisher K. E., Davis G. E., Cornelison D. D., 3D timelapse analysis of muscle satellite cell motility. Stem Cells 27, 2527–2538 (2009). [DOI] [PMC free article] [PubMed] [Google Scholar]

30. Eming S. A., Krieg T., Davidson J. M., Inflammation in wound repair: Molecular and cellular mechanisms. J. Invest. Dermatol. 127, 514–525 (2007). [DOI] [PubMed] [Google Scholar]

31. Bordoni B., Zanier E., Skin, fascias, and scars: Symptoms and systemic connections. J. Multidiscip. Healthc. 7, 11–24 (2013). [DOI] [PMC free article] [PubMed] [Google Scholar]

32. Rompolas P., Deschene E. R., Zito G., Gonzalez D. G., Saotome I., Haberman A. M., Greco V., Live imaging of stem cell and progeny behaviour in physiological hair-follicle regeneration. Nature 487, 496–499 (2012). [DOI] [PMC free article] [PubMed] [Google Scholar]

33. Yin H., Price F., Rudnicki M. A., Satellite cells and the muscle stem cell niche. Physiol. Rev. 93, 23–67 (2013). [DOI] [PMC free article] [PubMed] [Google Scholar]

34. Wang Y. X., Rudnicki M. A., Satellite cells, the engines of muscle repair. Nat. Rev. Mol. Cell Biol. 13, 127–133 (2011). [DOI] [PubMed] [Google Scholar]

35. Basak O., Born M., Korving J., Beumer J., Elst S., Es J. H., Clevers H., Mapping early fate determination in Lgr5^{+} crypt stem cells using a novel Ki67-RFP allele. EMBO J. 33, 2057–2068 (2014). [DOI] [PMC free article] [PubMed] [Google Scholar]

36. Rocheteau P., Gayraud-Morel B., Siegl-Cachedenier I., Blasco M. A., Tajbakhsh S., A subpopulation of adult skeletal muscle stem cells retains all template DNA strands after cell division. Cell 148, 112–125 (2012). [DOI] [PubMed] [Google Scholar]

37. Rodgers J. T., King K. Y., Brett J. O., Cromie M. J., Charville G. W., Maguire K. K., Brunson C., Mastey N., Liu L., Tsai C. R., Goodell M. A., Rando T. A., mTORC1 controls the adaptive transition of quiescent stem cells from G_0 to G_{Alert}. Nature 510, 393–396 (2014). [DOI] [PMC free article] [PubMed] [Google Scholar]

38. Song Y., Li D., Farrelly O., Miles L., Li F., Kim S. E., Lo T. Y., Wang F., Li T., Thompson-Peer K. L., Gong J., Murthy S. E., Coste B., Yakubovich N., Patapoutian A., Xiang Y., Rompolas P., Jan L. Y., Jan Y. N., The mechanosensitive ion channel Piezo inhibits axon regeneration. Neuron 102, 373–389.e6 (2019). [DOI] [PMC free article] [PubMed] [Google Scholar]

39. Tsuchiya M., Hara Y., Okuda M., Itoh K., Nishioka R., Shiomi A., Nagao K., Mori M., Mori Y., Ikenouchi J., Suzuki R., Tanaka M., Ohwada T., Aoki J., Kanagawa M., Toda T., Nagata Y., Matsuda R., Takayama Y., Tominaga M., Umeda M., Cell surface flip-flop of phosphatidylserine is critical for PIEZO1-mediated myotube formation. Nat. Commun. 9, 2049 (2018). [DOI] [PMC free article] [PubMed] [Google Scholar]

40. Syeda R., Xu J., Dubin A. E., Coste B., Mathur J., Huynh T., Matzen J., Lao J., Tully D. C., Engels I. H., Petrassi H. M., Schumacher A. M., Montal M., Bandell M., Patapoutian A., Chemical activation of the mechanotransduction channel Piezo1. eLife 4, (2015). [DOI] [PMC free article] [PubMed] [Google Scholar]

41. Cahalan S. M., Lukacs V., Ranade S. S., Chien S., Bandell M., Patapoutian A., Piezo1 links mechanical forces to red blood cell volume. eLife 4, (2015). [DOI] [PMC free article] [PubMed] [Google Scholar]

42. Madisen L., Zwingman T. A., Sunkin S. M., Oh S. W., Zariwala H. A., Gu H., Ng L. L., Palmiter R. D., Hawrylycz M. J., Jones A. R., Lein E. S., Zeng H., A robust and high-throughput Cre reporting and characterization system for the whole mouse brain. Nat. Neurosci. 13, 133–140 (2010). [DOI] [PMC free article] [PubMed] [Google Scholar]

43. Murphy M. M., Lawson J. A., Mathew S. J., Hutcheson D. A., Kardon G., Satellite cells, connective tissue fibroblasts and their interactions are crucial for muscle regeneration. Development 138, 3625–3637 (2011). [DOI] [PMC free article] [PubMed] [Google Scholar]

44. Emery A. E., Muscular dystrophy into the new millennium. Neuromuscul. Disord. 12, 343–349 (2002). [DOI] [PubMed] [Google Scholar]

45. Dumont N. A., Wang Y. X., von Maltzahn J., Pasut A., Bentzinger C. F., Brun C. E., Rudnicki M. A., Dystrophin expression in muscle stem cells regulates their polarity and asymmetric division. Nat. Med. 21, 1455–1463 (2015). [DOI] [PMC free article] [PubMed] [Google Scholar]

46. Im W. B., Phelps S. F., Copen E. H., Adams E. G., Slightom J. L., Chamberlain J. S., Differential expression of dystrophin isoforms in strains of mdx mice with different mutations. Hum. Mol. Genet. 5, 1149–1153 (1996). [DOI] [PubMed] [Google Scholar]

47. Inaba M., Buszczak M., Yamashita Y. M., Nanotubes mediate niche-stem-cell signalling in the Drosophila testis. Nature 523, 329–332 (2015). [DOI] [PMC free article] [PubMed] [Google Scholar]

48. Jaafar Marican N. H., Cruz-Migoni S. B., Borycki A. G., Asymmetric distribution of primary cilia allocates satellite cells for self-renewal. Stem Cell Rep. 6, 798–805 (2016). [DOI] [PMC free article] [PubMed] [Google Scholar]

49. Kryvi H., The structure of the myosatellite cells in axial muscles of the shark *Geleus melastomus*. Anat. Embryol. 147, 35–44 (1975). [DOI] [PubMed] [Google Scholar]

50. Larocque A. A., Politoff A. L., Peters A., The visualization of myosatellite cells in normal and denervated muscle: A new light microscopic staining technique. Anat. Rec. 196, 373–385 (1980). [DOI] [PubMed] [Google Scholar]

51. Oikawa T., Oyama M., Kozuka-Hata H., Uehara S., Udagawa N., Saya H., Matsuo K., Tks5-dependent formation of circumferential podosomes/invadopodia mediates cell-cell fusion. J. Cell Biol. 197, 553–568 (2012). [DOI] [PMC free article] [PubMed] [Google Scholar]

52. Short B., Protrusion drives osteoclast fusion. J. Cell Biol. 197, 460 (2012). [Google Scholar]

53. Obermann J., Wagner F., Kociaj A., Zambusi A., Ninkovic J., Hauck S. M., Chapouton P., The surface proteome of adult neural stem cells in zebrafish unveils long-range cell-cell connections and age-related changes in responsiveness to IGF. Stem Cell Rep. 12, 258–273 (2019). [DOI] [PMC free article] [PubMed] [Google Scholar]

54. Eng C. L., Lawson M., Zhu Q., Dries R., Koulena N., Takei Y., Yun J., Cronin C., Karp C., Yuan G.-C., Cai L., Transcriptome-scale super-resolved imaging in tissues by RNA seqFISH. Nature 568, 235–239 (2019). [DOI] [PMC free article] [PubMed] [Google Scholar]

55. Rodriques S. G., Stickels R. R., Goeva A., Martin C. A., Murray E., Vanderburg C. R., Welch J., Chen L. M., Chen F., Macosko E. Z., Slide-seq: A scalable technology for measuring genome-wide expression at high spatial resolution. Science 363, 1463–1467 (2019). [DOI] [PMC free article] [PubMed] [Google Scholar]

56. Voog J., Jones D. L., Stem cells and the niche: A dynamic duo. Cell Stem Cell 6, 103–115 (2010). [DOI] [PMC free article] [PubMed] [Google Scholar]

57. Joe A. W., Yi L., Natarajan A., Grand F. L., So L., Wang J., Rudnicki M. A., Rossi F. M. V., Muscle injury activates resident fibro/adipogenic progenitors that facilitate myogenesis. Nat. Cell Biol. 12, 153–163 (2010). [DOI] [PMC free article] [PubMed] [Google Scholar]

58. Lemos D. R., Babaeijandaghi F., Low M., Chang C. K., Lee S. T., Fiore D., Zhang R. H., Natarajan A., Nedospasov S. A., Rossi F. M. V., Nilotinib reduces muscle fibrosis in chronic muscle injury by promoting TNF-mediated apoptosis of fibro/adipogenic progenitors. Nat. Med. 21, 786–794 (2015). [DOI] [PubMed] [Google Scholar]

59. Afshar Bakooshli M., Lippmann E. S., Mulcahy B., Iyer N., Nguyen C. T., Tung K., Stewart B. A., van den Dorpel H., Fuehrmann T., Shoichet M., Bigot A., Pegoraro E., Ahn H., Ginsberg H., Zhen M., Ashton R. S., Gilbert P. M., A 3D culture model of innervated human skeletal muscle enables studies of the adult

neuromuscular junction. eLife 8, (2019). [DOI] [PMC free article] [PubMed] [Google Scholar]

60. Larouche J. A., Mohiuddin M., Choi J. J., Ulintz P. J., Fraczek P., Sabin K., Pitchiaya S., Kurpiers S. J., Castor-Macias J., Liu W., Hastings R. L., Brown L. A., Markworth J. F., de Silva K., Levi B., Merajver S. D., Valdez G., Chakkalakal J. V., Jang Y. C., Brooks S. V., Aguilar C. A., Murine muscle stem cell response to perturbations of the neuromuscular junction are attenuated with aging. eLife 10, (2021). [DOI] [PMC free article] [PubMed] [Google Scholar]

61. Murthy S. E., Dubin A. E., Patapoutian A., Piezos thrive under pressure: Mechanically activated ion channels in health and disease. Nat. Rev. Mol. Cell Biol. 18, 771–783 (2017). [DOI] [PubMed] [Google Scholar]

62. Sun W., Chi S., Li Y., Ling S., Tan Y., Xu Y., Jiang F., Li J., Liu C., Zhong G., Cao D., Jin X., Zhao D., Gao X., Liu Z., Xiao B., Li Y., The mechanosensitive Piezo1 channel is required for bone formation. eLife 8, (2019). [DOI] [PMC free article] [PubMed] [Google Scholar]

63. Jiang F., Yin K., Wu K., Zhang M., Wang S., Cheng H., Zhou Z., Xiao B., The mechanosensitive Piezo1 channel mediates heart mechano-chemo transduction. Nat. Commun. 12, 869 (2021). [DOI] [PMC free article] [PubMed] [Google Scholar]

64. K. Hirano, M. Tsuchiya, S. Takabayashi, K. Nagao, Y. Kitajima, Y. Ono, K. Nonomura, Y. Mori, M. Umeda, Y. Hara, The mechanosensitive Ca^{2+}-permeable ion channel PIEZO1 promotes satellite cell function in skeletal muscle regeneration. bioRxiv 2021.03.18.435982 [**Preprint**]. 18 March 2021. 10.1101/2021.03.18.435982. [DOI]

65. Wang M. J., Zhu Y. C., Shi J., A crucial physiological role of Piezo1 channel in differentiation rather than proliferation during myogenesis. Acta Physiol. 233, e13728 (2021). [DOI] [PubMed] [Google Scholar]

66. Endow S. A., Miller S. E., Ly P. T., Mitochondria-enriched protrusions are associated with brain and intestinal stem cells in *Drosophila*. Commun. Biol. 2, 427 (2019). [DOI] [PMC free article] [PubMed] [Google Scholar]

Associated Data

This section collects any data citations, data availability statements, or supplementary materials included in this article.

Supplementary Materials

Figs. S1 to S10

Table S1

Click here for additional data file. (12.1MB, pdf)

Movies S1 to S5

Click here for additional data file. (27.6MB, zip)
